Croatian Society
for Materials
Protection

Metalurgija/Metallurgy

Vol. 66 No. 1 / 2027

Effect of Ultrasonic Surface Rolling on Tribological Properties of 7075 Aluminum Alloy for Yangqin Components

Yu Wang[1,*]

https://doi.org/10.64486/m.66.1.14

[1] Harbin University, Harbin City, No. 108, Sanfu Street, Xiangfang District, Harbin City, Heilongjiang Province, China, 150086
* Correspondence: 18946114323@163.com

Type of the Paper: Article
Received: May 24, 2026
Accepted: July 15, 2026

Abstract: Lightweight metallic parts considered for auxiliary tuning or moving hardware in Yangqin instruments may experience sliding or rotational contact and therefore require adequate wear resistance. This study treats Yangqin as a potential application background and investigates 7075-T6 aluminum alloy after ultrasonic surface rolling process (USRP) under simplified laboratory contact conditions. Static pressure, rolling speed, indentation depth and rolling passes were evaluated, and rotational and reciprocating ball-on-disk tests were used as representative sliding modes rather than component-level validation. A rolling speed of 2000 mm/min, static pressure of 300 N, indentation depth of 0.10 mm and 8 passes produced a gradient nanostructured layer about 114 μm thick. Under these conditions, *Ra* decreased to (0.240 ± 0.009) μm and near-surface hardness increased to (230 ± 14) HV. The maximum numerical wear-volume reduction was 40.9 % in rotational sliding at 5 N and 41.0 % in reciprocating sliding at 10 N. ANOVA confirmed significant rotational wear-volume effects at 5 N and 10 N and a significant reciprocating effect at 10 N; lower-load trends were not significant. The optimized USRP condition promoted a more stable mechanical mixing layer and improved materials-level wear performance, providing a basis for future validation on Yangqin-related components.

Keywords: Yangqin; aluminum alloy; ultrasonic surface rolling process; friction and wear

1. Introduction

Yangqin is a Chinese hammered dulcimer played by striking metal strings with handheld hammers; its structure includes strings, bridges, tuning pins and fine-tuning hardware [1]. In generic mechanical contacts, repeated small-amplitude relative motion can cause frictional damage and progressively alter local contact geometry [2]. Accordingly, metallic materials considered for auxiliary tuning or moving hardware require adequate surface wear resistance. Because actual Yangqin component geometry, contact pairs, lubrication state and load spectra are complex, the present work does not claim direct component-level verification. Instead, it uses Yangqin as a potential application background and evaluates the wear resistance of a candidate lightweight alloy under simplified laboratory contact modes.

Aluminum alloy has the advantages of high specific strength, low density, good corrosion resistance and excellent processability, and has been widely used in structural parts in aerospace, automotive manufacturing and other fields [4-5]. Among these alloys, 7075-T6 aluminum alloy has high strength and low density, making it a potential candidate material for lightweight Yangqin structural or moving components. However, 7075 aluminum alloy has relatively low surface hardness (about 180 HV) and poor wear resistance, and is prone to surface damage under dry sliding contact, which limits its direct use in moving components [6]. Therefore, developing efficient surface modification technologies to improve the wear resistance of 7075 aluminum alloy is meaningful for both general mechanical applications and potential musical-instrument components.

At present, surface modification methods to improve the wear resistance of aluminum alloy mainly include particle reinforcement composite, chemical heat treatment and severe plastic deformation (SPD) technology. The particle reinforcement composite method improves the hardness by introducing hard particles such as SiC and Al_2O_3 into the aluminum alloy surface, but it has the problems of poor interface bonding, complex process and high cost [7-8]. Chemical heat treatments such as nitriding and boronizing can significantly improve the surface hardness, but they require high treatment temperature and long cycle time, which easily lead to the degradation of the mechanical properties of the aluminum alloy matrix [9-10]. In contrast, SPD technology achieves grain refinement by introducing large plastic deformation on the material surface, which can simultaneously improve the surface hardness and toughness without changing the chemical composition of the material, while maintaining the good properties of the matrix [9]. Typical SPD methods include laser shock peening (LSP), ultrasonic shot peening (USSP), equal channel angular pressing (ECAP) and ultrasonic surface rolling process (USRP). Among them, USRP combines traditional rolling and ultrasonic vibration technology, which can form a gradient nanostructure on the material surface and significantly reduce the surface roughness, making it a surface modification technology with great industrial application prospects [11-13].

In recent years, extensive research has been conducted on the application of USRP to the surface modification of metallic materials. Xiong et al. prepared a deformation layer with a thickness of about 400 μm and a nanostructured layer of about 20 μm on the surface of 7075 aluminum alloy by USRP, which increased the tensile strength while maintaining good ductility [11]. Sun et al. found that USRP treatment significantly improved the corrosion resistance of 7075 aluminum alloy [12]. In tribology, Ye et al. treated QAl10-3-1.5 aluminum bronze alloy with USRP and found that the surface grains were refined to nanoscale and the wear resistance was markedly improved [13]. Chen et al. reported that USRP reduced the friction coefficient and wear volume of uranium samples [14], and Wang et al. showed that a USRP-induced gradient nanostructure in M50 bearing steel inhibited crack propagation [15]. For 7075 aluminum alloy, Zhou et al. demonstrated that ultrasonic-assisted surface burnishing improved wear resistance under low load [16]. These studies indicate that grain refinement, hardness improvement, residual-stress regulation and mechanical mixing-layer formation are closely related to the tribological performance of USRP-treated metals.

However, the connection between USRP-treated 7075 aluminum alloy and the service behavior of actual Yangqin moving components remains insufficiently validated. To avoid overextending the application claim, this paper presents a materials-level laboratory investigation. USRP was used to modify the surface of 7075-T6 aluminum alloy; the process parameters including static pressure, rolling speed, indentation depth and rolling passes were optimized; and rotational and reciprocating dry sliding tests were selected to qualitatively represent two common forms of relative motion. Finally, combined with microstructure and worn-surface characterization, the mechanism by which USRP improves the wear resistance of 7075 aluminum alloy was discussed. Future work should further verify the process on representative Yangqin components with realistic geometry, load spectrum and acoustic-performance requirements.

https://doi.org/10.64486/m.66.1.14

2. Materials and Methods

2.1. Experimental Materials and Instruments

Commercial 7075-T6 aluminum alloy bar was selected as a candidate lightweight material for potential auxiliary Yangqin components, and its chemical composition is shown in Table 1. Disc samples with dimensions of Ø 40 mm × 6 mm were cut from the bar using an electrical discharge wire cutter. The samples were mechanically ground sequentially with 220#, 400#, 800#, 1200# and 2000# silicon carbide sandpapers, then ultrasonically cleaned with ethanol for 3 min and blown dry with cold air for later use.

Table 1. Chemical composition of 7075-T6 aluminum alloy (wt. %)

Material	Zn	Mg	Cu	Fe	Si	Cr	Al
7075-T6	5.2	2.52	1.63	0.5	0.4	0.18	Balance

2.2. Experimental Equipment and Test Methods

2.2.1. Ultrasonic Surface Rolling Treatment

USRP treatment was carried out on a USM-300 CNC machine tool. A WC-Co cemented carbide ball with a diameter of 14 mm was used as the rolling head. The fixed process parameters were vibration frequency 27 kHz, amplitude 10 μm and oil lubrication. To optimize the process parameters, the effects of static pressure (165 N, 230 N, 300 N and 400 N), rolling speed (1000, 1500, 2000, 2500 and 3000 mm/min) and indentation depth (0.02 mm, 0.05 mm, 0.10 mm and 0.20 mm) on surface properties were investigated. Based on the comparative metallographic and roughness results, the subsequent rolling-pass tests used 2000 mm/min rolling speed, 300 N static pressure and 0.10 mm indentation depth, with 2, 5 and 8 rolling passes. The untreated sample was marked as the CG sample.

2.2.2. Microstructure Characterization

An SPD TOP ICX41M optical microscope (OM) was used to observe the cross-sectional microstructure of the samples. The samples were embedded in epoxy resin, ground with sandpapers, mechanically polished, and then etched with Keller's reagent (1 mL HF + 1.5 mL HCl + 2.5 mL HNO_3 + 95 mL H_2O) for 90 s. A LEXT OLS4000 laser confocal scanning microscope (CLSM) and a Bruker Contour GT-K white light interferometer were used to analyze the surface morphology and roughness. A ZEISS SUPRA55 field emission scanning electron microscope (SEM) was used to observe the worn surface morphology, equipped with an AZtecSynergy microanalysis system for energy dispersive spectroscopy (EDS) analysis. A FEI Talos F200X transmission electron microscope (TEM) was used to observe the surface microstructure, and TEM samples were prepared by focused ion beam (FIB) technology.

2.2.3. Friction and Wear Test

Friction and wear tests were carried out on an Rtec MFT-5000 multifunctional friction and wear tester using a ball-on-disk contact mode. The counterbody was a WC-Co cemented carbide ball with a diameter of 9.625 mm. The experiments were designed as simplified material-level tests: rotational and reciprocating sliding were used as two representative relative-motion modes relevant to potential auxiliary Yangqin components, but the tests do not reproduce actual component geometry, assembly clearance, impact loading or acoustic response.

- Rotational friction test parameters: linear velocity 0.025 m/s, time 30 min, loads 3 N, 5 N, 10 N
- Reciprocating friction test parameters: stroke 5 mm, frequency 1 Hz, time 30 min, loads 3 N, 5 N, 10 N

All experiments were conducted under room temperature (25 °C) dry friction conditions. After the experiments, the three-dimensional morphology of the wear tracks was measured using a white light interferometer, and the wear volume was calculated by integrating the wear-track cross-sectional area along the sliding path.

https://doi.org/10.64486/m.66.1.14

2.2.4. Statistical Analysis

Surface roughness and near-surface microhardness were measured at five locations per group and are reported as mean ± standard deviation (SD; $n = 5$). Each friction condition was independently repeated three times ($n = 3$). For each run, the time-averaged coefficient of friction (COF) over the full 1800 s test was calculated, and the three run-specific values were used to obtain the group mean ± SD. Ten cross-sectional profiles were measured on each wear track and averaged to obtain one wear-volume value for that independent run; wear-volume SD was then calculated across the three runs. The COF-time curve shown for each condition is the run closest to the corresponding group mean and is presented as a representative curve. For scalar endpoints, differences among CG, USRP(2), USRP(5) and USRP(8) were evaluated separately at each load and sliding mode using one-way analysis of variance (ANOVA) followed by Tukey's honestly significant difference test. A value of $p < 0.05$ was considered statistically significant.

3. Results and Discussion

3.1. Effect of USRP Process Parameters on Surface Morphology and Roughness of 7075 Aluminum Alloy

The cross-sectional metallographic images of 7075 aluminum alloy after USRP treatment under different static pressures are shown in Figure 1. All samples showed obvious plastic deformation layers in the subsurface (as shown in Figures a–d). At a static pressure of 165 N (Figure a), the indentation depth of the rolling body into the material surface was small, and only slightly curved flow lines were observed on the sample surface, with relatively coarse grains. When the static pressure increased to 230 N (Figure b), the curved flow lines on the surface became obvious, but the thickness of the deformation layer was small, about 70 μm. Figure c shows the metallographic structure at a static pressure of 300 N. It can be seen that the metal flow lines on the surface were significantly curved, the grains were refined, and the thickness of the deformation layer was about 75 μm. With further increase of static pressure to 400 N, irregular textures appeared on the sample surface, the surface became obviously rough, and cracks were generated in the deformation layer of the sample surface. Relevant literature shows that surface cracks are detrimental to the friction properties of materials. It can be seen that under the same rolling passes, the deformation effect at 300 N static pressure is optimal.

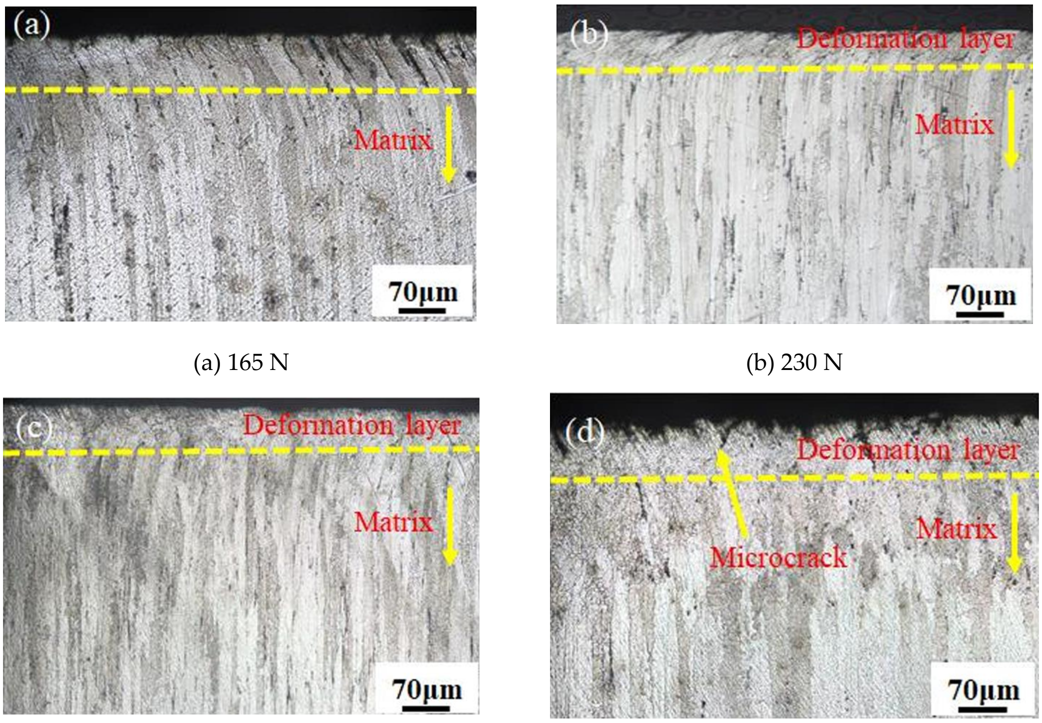

(a) 165 N (b) 230 N

(c) 300 N (d) 400 N

Figure 1. Cross-sectional metallographic images of samples under different static pressures

https://doi.org/10.64486/m.66.1.14

The cross-sectional metallographic images of 7075 aluminum alloy after USRP treatment under different indentation depths are shown in Figure 2. It can be seen from the figure that the surface morphology of USRP-treated samples varies significantly with different indentation depths. At an indentation depth of 0.02 mm (Figure a), slightly curved flow lines appeared on the surface, and the grains were still relatively coarse. When the indentation depth increased to 0.05 mm, the surface grains were obviously refined, and microcracks appeared in the subsurface as shown in Figure 2(b). After the indentation depth increased to 0.1 mm, the grain size decreased significantly, and the thickness of the plastic deformation layer was about 80 μm. When the indentation depth continued to increase to 0.2 mm, microcracks began to appear on the sample surface, and the thickness of the deformation layer decreased to 65 μm, the surface roughness increased, and spalling occurred in the deformation layer of the sample surface. It can be seen that under the same rolling passes, the deformation effect at an indentation depth of 0.1 mm is optimal.

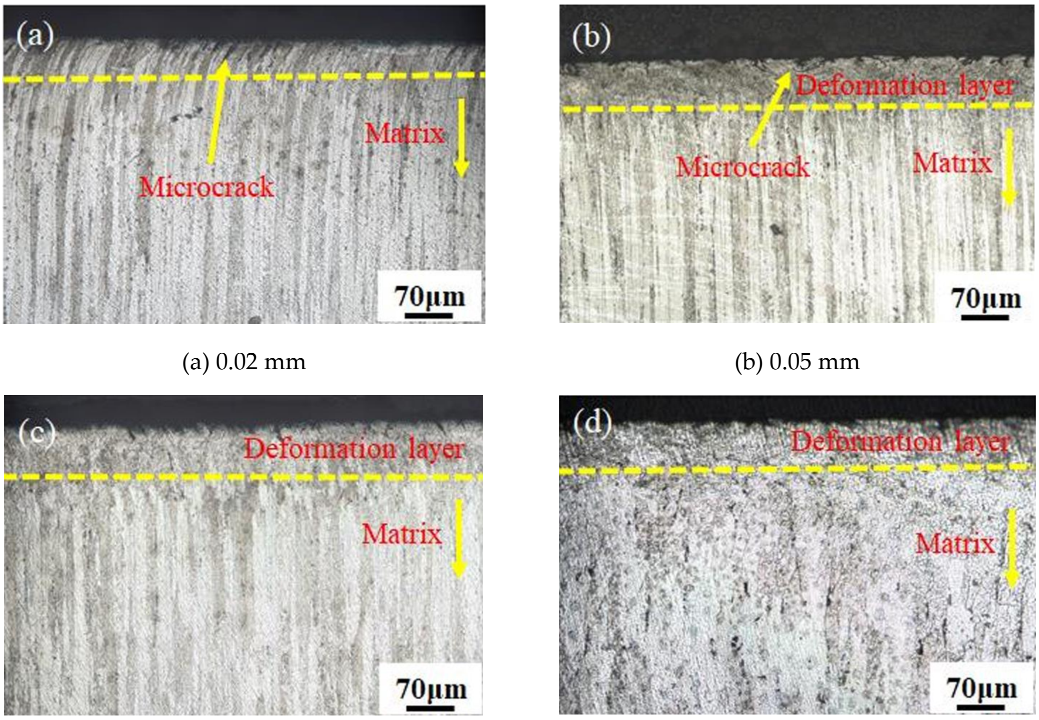

(a) 0.02 mm (b) 0.05 mm

(c) 0.1 mm (d) 0.2 mm

Figure 2. Cross-sectional metallographic images of samples under different indentation depths

Figure 3 shows the influence law of USRP treatment on the surface roughness of 7075 aluminum alloy. For comparison, the untreated sample (CG sample) was tested under the same conditions. It can be seen that the CG sample without USRP treatment had the roughest surface, and the surface roughness value of the aluminum alloy was significantly reduced after USRP treatment. It can be seen from Figure 3(a) that when the rolling speed reached 2000 mm/min, the fluctuation of the surface roughness curve of the sample became smaller and the surface roughness value was the lowest.

However, when the rolling speed reached 2500 mm/min, the fluctuation of the surface roughness curve began to increase again. This is because when the rolling speed reaches a certain level, the plastic deformation generated presses the peaks into the valleys. After the rolling speed increases further, some residual peaks are not sufficiently affected by ultrasonic vibration, resulting in increased residual height and re-roughening of the surface. Figure 3(b) shows the variation of the surface roughness curves under different static pressures. The surface roughness first decreases and then increases with increasing static pressure.

When the static pressure is small, the indentation depth of the rolling body is insufficient and no obvious plastic deformation is generated, so the surface quality improvement is not obvious. When the static pressure increased to 300 N, the roughness curve became relatively gentle and the surface state was optimal. When the static pressure increased to 400 N, the surface roughness increased because excessive indentation caused plastic-deformation accumulation and microcrack initiation. This is consistent with the results in Figure 1. Therefore, rolling speed of 2000 mm/min and static pressure of 300 N were selected for subsequent research.

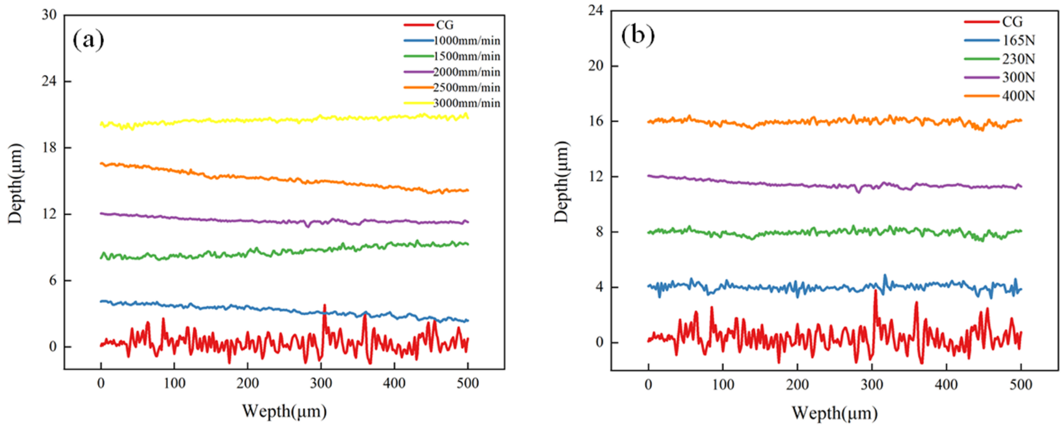

(a) Different rolling speeds (b) Different static pressures

Figure 3. Surface roughness curves

The scalar surface-property results under the selected process parameters are summarized in Table 2. One-way ANOVA showed significant group effects for *Ra* ($F(3,16) = 701.32$, $p < 0.001$), *Rq* ($F(3,16) = 665.99$, $p < 0.001$) and near-surface microhardness ($F(3,16) = 17.78$, $p < 0.001$). Tukey testing separated all four *Ra* and *Rq* means; the CG hardness was lower than every USRP group, while the three USRP hardness means were not significantly different from one another.

Table 2. Surface roughness and near-surface microhardness of CG and USRP-treated samples.

Sample	*Ra* / μm	*Rq* / μm	Near-surface microhardness / HV
CG	0.910 ± 0.046^{a}	1.120 ± 0.054^{a}	180 ± 8^{b}
USRP(2)	0.495 ± 0.014^{b}	0.698 ± 0.028^{b}	210 ± 12^{a}
USRP(5)	0.330 ± 0.011^{c}	0.380 ± 0.019^{c}	220 ± 11^{a}
USRP(8)	0.240 ± 0.009^{d}	0.290 ± 0.013^{d}	230 ± 14^{a}

Note: Values are presented as mean ± SD ($n = 5$). Different superscript letters within the same column indicate statistically significant differences according to Tukey's HSD test ($p < 0.05$). Values sharing at least one letter are not significantly different.

3.2. Effect of USRP Treatment on Friction and Wear Properties of 7075 Aluminum Alloy

Figures 4(a)-(c) show representative rotational COF-time curves. All curves exhibit a low-value period, a running-in period and a later quasi-steady period. Increasing the number of rolling passes generally prolonged the low-COF period and reduced the time-averaged COF. From CG to USRP(8), mean COF decreased from 0.460 ± 0.023 to 0.370 ± 0.020 at 3 N (19.6 %), from 0.460 ± 0.020 to 0.400 ± 0.022 at 5 N (13.0 %), and from 0.480 ± 0.019 to 0.400 ± 0.022 at 10 N (16.7 %). Figure 4(d) presents the corresponding wear volumes. The CG-to-USRP(8) reduction was 18.7 % at 3 N, 40.9 % at 5 N and 33.0 % at 10 N.

https://doi.org/10.64486/m.66.1.14

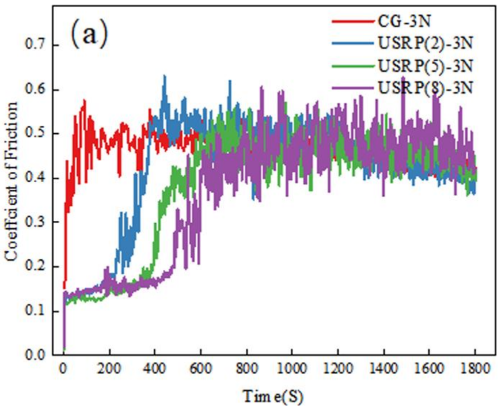

(a) 3 N

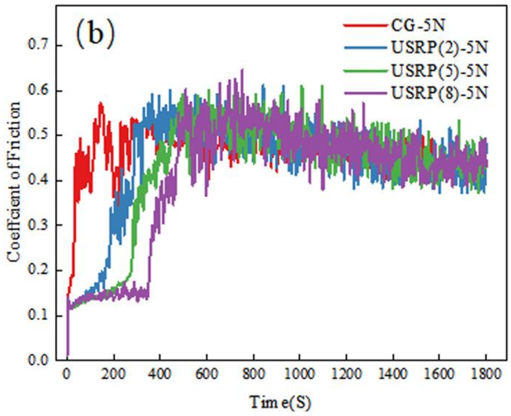

(b) 5 N

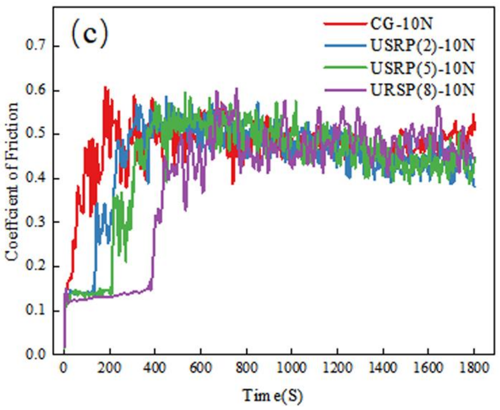

(c) 10 N

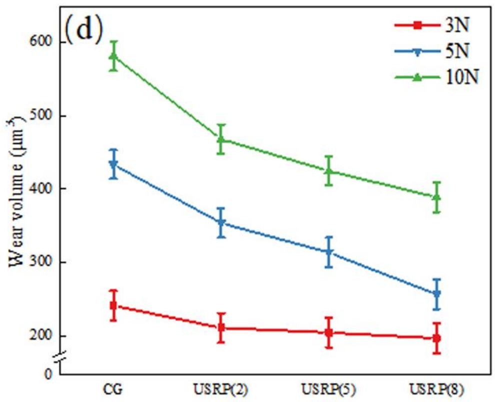

(d) Wear volume

Figure 4. Representative rotational COF-time curves and wear-volume results under different loads. Panels (a)-(c) are representative curves selected from the run closest to the group mean; error bars in panel (d) represent SD (n = 3). Statistical comparisons are reported in Table 3.

Table 3 reports the scalar rotational-sliding results and Tukey groupings. Group effects on mean COF were significant at 3 N ($F(3,8) = 8.39$, $p = 0.0075$), 5 N ($F(3,8) = 4.53$, $p = 0.0389$) and 10 N ($F(3,8) = 7.91$, $p = 0.0089$). The wear-volume effect was not significant at 3 N ($F(3,8) = 3.55$, $p = 0.0673$), but was significant at 5 N ($F(3,8) = 51.84$, $p < 0.001$) and 10 N ($F(3,8) = 60.86$, $p < 0.001$).

Table 3. Rotational sliding results under different normal loads.

Load / N	Sample	Time-averaged COF	Wear volume / μm³
3	CG	0.460 ± 0.023^{a}	241 ± 20^{a}
3	USRP(2)	0.420 ± 0.022^{ab}	211 ± 18^{a}
3	USRP(5)	0.400 ± 0.025^{b}	204 ± 18^{a}
3	USRP(8)	0.370 ± 0.020^{b}	196 ± 16^{a}
5	CG	0.460 ± 0.020^{a}	433 ± 19^{a}
5	USRP(2)	0.430 ± 0.021^{ab}	354 ± 20^{b}
5	USRP(5)	0.410 ± 0.023^{ab}	315 ± 17^{b}

https://doi.org/10.64486/m.66.1.14

Load / N	Sample	Time-averaged COF	Wear volume / μm³
5	USRP(8)	0.400 ± 0.022^{b}	256 ± 15^{c}
10	CG	0.480 ± 0.019^{a}	581 ± 20^{a}
10	USRP(2)	0.460 ± 0.022^{a}	466 ± 20^{b}
10	USRP(5)	0.440 ± 0.021^{ab}	423 ± 18^{bc}
10	USRP(8)	0.400 ± 0.022^{b}	389 ± 16^{c}

Note: Values are presented as mean ± SD (n = 3). Different superscript letters within the same column and at the same load indicate statistically significant differences according to Tukey's HSD test ($p < 0.05$). Values sharing at least one letter are not significantly different.

The surface wear morphologies of CG samples after sliding friction for 1 min, 7 min and 30 min under friction forces of 3 N, 5 N and 10 N are shown in Figure 5. After 1 min of sliding, due to the rapid increase of the friction coefficient of the CG sample, its wear characteristics were only some compacted wear debris, and the entire worn surface was smooth. With the increase of time to 7 min, the friction coefficient became stable, the strain rate near the worn surface during friction became high, and some wear debris was re-pressed into the friction pair. These wear debris formed by surface fracture and some fine wear debris were distributed on the surface.

The newly generated wear debris had extremely high surface energy, and the contact area underwent severe deformation during friction. However, no high temperature rise was generated during this process, so the newly generated surface area was not easily oxidized, and obvious adhesive wear characteristics and furrows began to appear.

The main morphology of the worn surface was dominated by wear debris and a small amount of compacted wear debris. When the friction time increased to 30 min, the surface of the CG sample was mainly composed of oxygen-containing wear debris, and the wear characteristic of the entire sample was dominated by abrasive wear. It can be seen that with the increase of friction time, the accumulated plastic strain on the surface of the CG sample led to an increase in the protrusions on the wear track surface. These protrusions fractured under the action of shear stress, and at the same time, the surface roughness in the sliding direction increased, eventually leading to the shedding of the surface oxide layer.

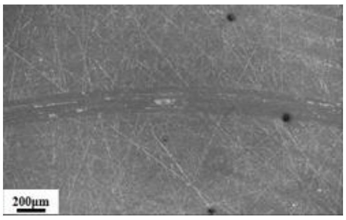

(a) 3 N–1 min

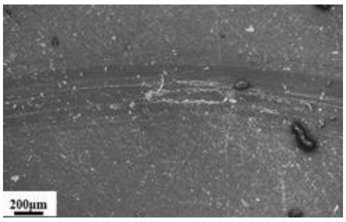

(b) 3 N–7 min

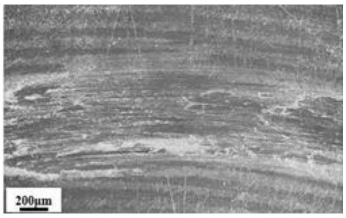

(c) 3 N–30 min

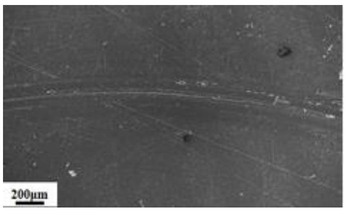

(d) 5 N–1 min

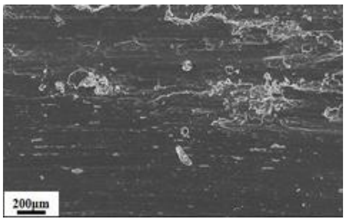

(e) 5 N–7 min

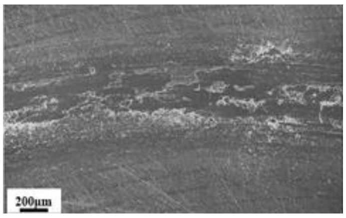

(f) 5 N–30 min

https://doi.org/10.64486/m.66.1.14

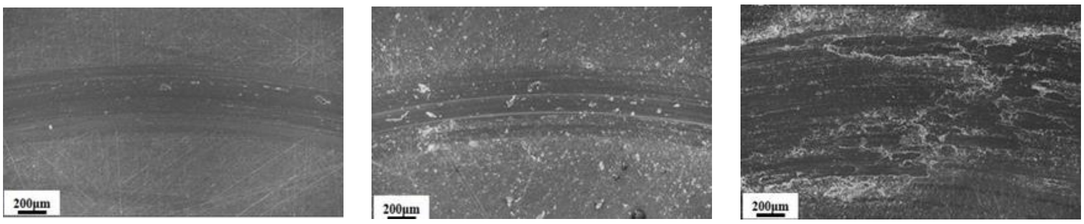

(g) 10 N–1 min (h) 10 N–7 min (i) 10 N–30 min

Figure 5. Friction and wear surface morphologies under different wear times and friction loads

The surface wear morphologies of USRP(2) sample after sliding friction for (1-30) min under 10 N friction force are shown in Figure 6. After 1 min of wear, a small amount of wear debris appeared on the surface. With the increase of friction time to 7 min, adhesive wear characteristics began to appear, accompanied by the generation of wear debris. Compared with the CG sample, the USRP(2) sample produced less wear debris and narrower wear tracks within the first 7 min of friction, which is related to the improvement of microhardness by the USRP process. When the friction time increased to 30 min, a large amount of wear debris was generated on the surface, and the wear characteristic of the entire sample was dominated by abrasive wear, accompanied by slight adhesive wear characteristics. Overall, the wear characteristics of USRP(2) sample and CG sample after 30 min under 10 N did not change significantly.

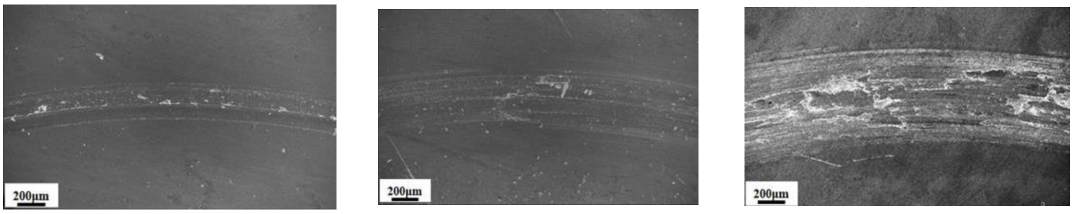

(a) 10 N–1 min (b) 10 N–7 min (c) 10 N–30 min

Figure 6. Friction and wear surface morphologies under different wear times

Figure 7 shows the friction and wear surface morphologies of USRP(5) sample under 10 N friction load for 1-30 min. Compared with the USRP(2) sample, there was no difference in the friction morphologies at 1 min and 7 min, which benefits from the gradient nanostructure introduced by USRP on the surface. The good subsurface layer can accommodate more plastic strain, and its wear characteristic is dominated by adhesive wear. When the friction time increased to 30 min, compared with CG sample and USRP(2) sample, the USRP(5) sample had fewer and smaller wear debris.

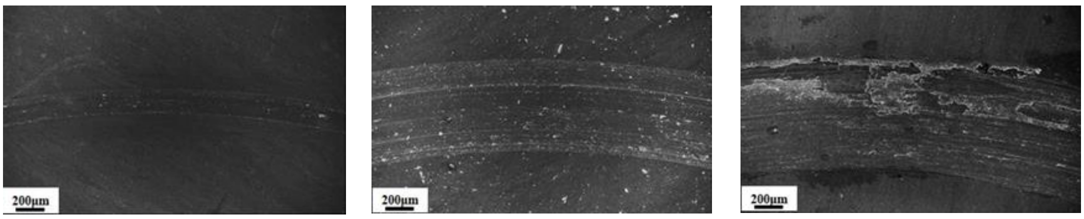

(a) 10N–1 min (b) 10N–7 min (c) 10N–30 min

Figure 7. Friction and wear surface morphologies under different wear times

The surface wear morphologies of USRP(8) sample after sliding friction for (1–30) min under 10 N friction force are shown in Figure 8. After 1 min of sliding, the friction coefficient did not increase rapidly, and some plowing marks were left on the surface along the friction direction, with almost no wear debris characteristics. With the increase of friction time, the friction coefficient also increased. The high shear stress during friction and wear led to fracture caused by adhesive wear on the surface, accompanied by the generation of some wear debris. At this time, part of the friction force was converted into the resistance between the compacted wear debris and the surface layer, accompanied by the change of the friction surface morphology. Compared with

 https://doi.org/10.64486/m.66.1.14

the CG sample, the surface wear characteristics of the USRP sample showed differences after 7 min of friction experiment, with significantly reduced wear debris, increased adhesive wear characteristics, and the beginning of the formation of a mechanical mixing layer. When the friction time increased to 30 min, the friction coefficient tended to be stable. Part of the wear track surface was covered by a rough oxide layer, and these oxides had very small grain sizes. At the same time, the main source of wear debris was the initiation and propagation of cracks in the oxide layer, and finally shedding. At this time, the main wear characteristic was adhesive wear.

It is well known that the wear resistance of materials mainly depends on the surface hardness of the materials. USRP treatment increases the hardness of the material. Under the same friction force, the higher the hardness, the better the wear resistance, and increasing the sliding speed during friction will not cause obvious damage to the surface layer. However, the CG sample has low hardness, and cracks are more easily formed on the surface layer under the same friction force, leading to surface spalling, so the wear resistance of the CG sample is poor. In the early running-in stage, the CG sample produced deeper wear track depth and more wear debris, which made the wear debris accumulate to the center of the deepest wear track under the action of friction force. The wear debris was oxidized, fragmented and agglomerated under the combined action of extrusion stress and friction heat, forming a brittle oxide layer. This eventually led to the rapid end of the running-in stage and the entry into the stable wear stage. For USRP samples, under the same friction conditions, the number and size of generated wear debris were smaller, and the generated wear tracks were shallower, which was conducive to the timely discharge of wear debris under the action of normal stress. These loose wear debris had certain mobility during the running-in stage, which resulted in lower COF of USRP samples during this stage. Therefore, USRP samples have a longer running-in period than CG samples, which is also the key to their excellent wear resistance.

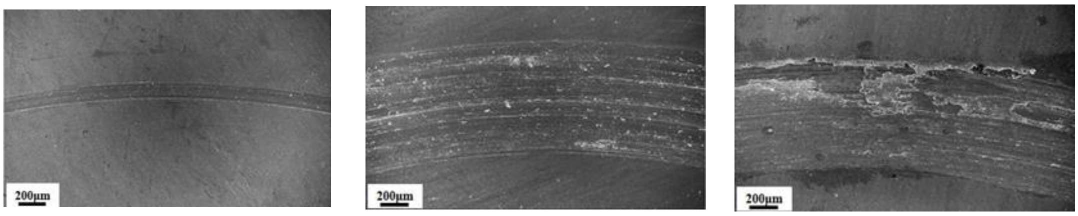

(a) 10 N–1 min (b) 10 N–7 min (c) 10 N–30 min

Figure 8. Friction and wear surface morphologies under different wear times

In addition, as shown in Figure 9, the TEM observations of the outermost surface layer of the USRP(8) sample before and after dry sliding wear reveal clear microstructural evolution. Before the wear test, abundant secondary phases were present within the surface grains and along the grain boundaries of the USRP(8) sample. After the wear test, the amount of secondary phases inside the grains decreased significantly, as shown in Figure 9(d). The color-coded high-resolution images in Figures 9(b) and 9(e) show that the red regions within the grains increased markedly after wear. The inverse fast Fourier transform (IFFT) results further indicate a significant increase in dislocation density, as shown in Figures 9(c) and 9(f). Specifically, the dislocation density of the nanolamellar structure in the USRP(8) sample before wear was 5.74×10^{15} m^{-2}, as shown in Figure 9(c), whereas it increased to 1.98×10^{16} m^{-2} after the wear test, as shown in Figure 9(f). The dislocation density in the amorphous structure reached 4.74×10^{16} m^{-2}, as shown in Figure 9(d). These results indicate that, during friction and wear, the USRP-treated sample undergoes further grain refinement and accumulates a higher density of dislocations.

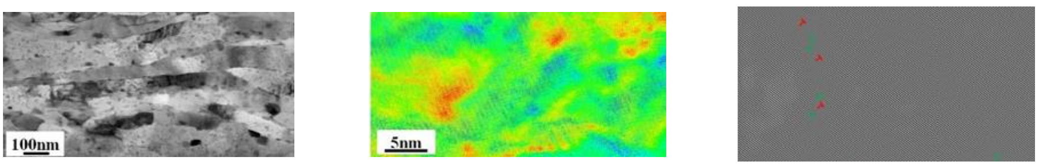

(a) bright-field image (b) HRTEM image (c) corresponding IFFT image of (b)

 https://doi.org/10.64486/m.66.1.14

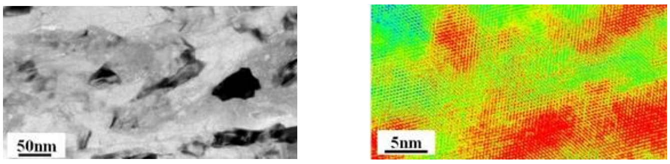

(d) bright-field image (e) HRTEM image (f) corresponding IFFT image of (e)

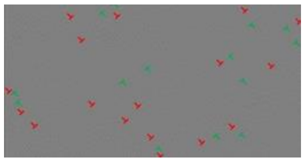

Figure 9. TEM images of the outermost surface layer of the USRP(8) sample before and after friction and wear

3.3. Reciprocating Friction Behavior

The reciprocating test was added to compare rotational sliding with repeated short-stroke motion that may occur in auxiliary mechanisms. From CG to USRP(8), the mean COF decreased from 0.450 ± 0.025 to 0.380 ± 0.021 at 3 N (15.6 %), from 0.450 ± 0.028 to 0.390 ± 0.023 at 5 N (13.3 %), and from 0.470 ± 0.026 to 0.400 ± 0.025 at 10 N (14.9 %). The corresponding wear volume decreased from 21 459 ± 3 216 to 14 071 ± 3 177 μm³ at 3 N, from 30 301 ± 3 309 to 24 511 ± 3 156 μm³ at 5 N, and from 83 426 ± 4 215 to 49 245 ± 4 872 μm³ at 10 N. The representative reciprocating COF-time curves and the corresponding wear-volume results are shown in Figure 10.

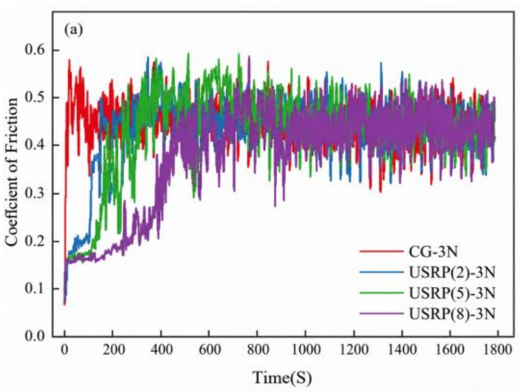

(a)3 N

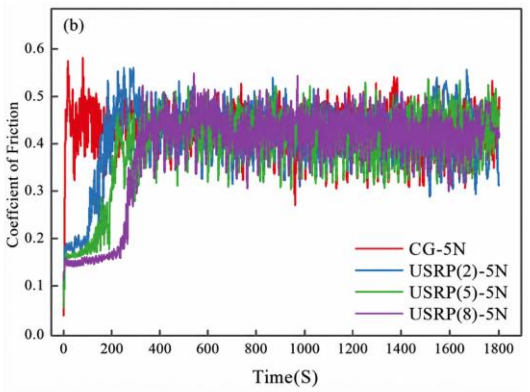

(b) 5 N

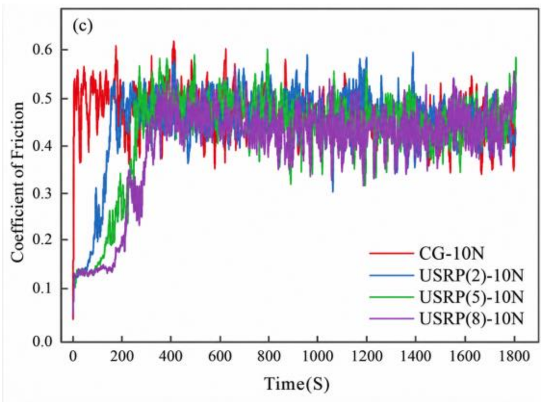

(c) 10 N

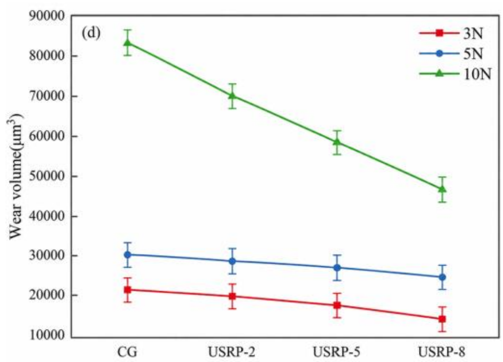

(d) Wear volume

Figure 10. Representative reciprocating COF-time curves and wear-volume results under different loads. Panels (a) – (c) are representative curves selected from the run closest to the group mean; error bars in panel (d) represent SD (n = 3). Statistical comparisons are reported in Table 4.

Table 4 summarizes the reciprocating results. Group effects on mean COF were significant at 3 N ($F(3,8) = 4.40$, $p = 0.0416$) and 10 N ($F(3,8) = 4.18$, $p = 0.0469$), but not at 5 N ($F(3,8) = 2.70$, $p = 0.1163$). Wear-volume effects

https://doi.org/10.64486/m.66.1.14

were not significant at 3 N ($F(3,8) = 2.99$, $p = 0.0959$) or 5 N ($F(3,8) = 1.53$, $p = 0.2791$), but were significant at 10 N ($F(3,8) = 31.16$, $p < 0.001$). At 10 N, Tukey testing showed that CG exceeded all USRP groups and USRP(8) was lower than USRP(2).

Table 4. Reciprocating sliding results under different normal loads.

Load / N	Sample	Time-averaged COF	Wear volume / μm³
3	CG	0.450 ± 0.025^{a}	21 459 ± 3 216^{a}
3	USRP(2)	0.420 ± 0.023^{ab}	19 600 ± 3 267^{a}
3	USRP(5)	0.410 ± 0.026^{ab}	17 500 ± 3 033^{a}
3	USRP(8)	0.380 ± 0.021^{b}	14 071 ± 3 177^{a}
5	CG	0.450 ± 0.028^{a}	30 301 ± 3 309^{a}
5	USRP(2)	0.430 ± 0.025^{a}	28 600 ± 3 516^{a}
5	USRP(5)	0.420 ± 0.029^{a}	27 000 ± 3 768^{a}
5	USRP(8)	0.390 ± 0.023^{a}	24 511 ± 3 156^{a}
10	CG	0.470 ± 0.026^{a}	83 426 ± 4 215^{a}
10	USRP(2)	0.450 ± 0.027^{ab}	70 000 ± 4 695^{b}
10	USRP(5)	0.430 ± 0.023^{ab}	58 500 ± 4 526^{bc}
10	USRP(8)	0.400 ± 0.025^{b}	49 245 ± 4 872^{c}

Note: Values are presented as mean ± SD ($n = 3$). Different superscript letters within the same column and at the same load indicate statistically significant differences according to Tukey's HSD test ($p < 0.05$). Values sharing at least one letter are not significantly different.

Compared with rotational sliding, reciprocating wear volume was much larger because reversal promotes stress concentration, debris accumulation and repeated re-entry of wear particles into the contact zone. The numerical reductions at 3 N and 5 N did not reach statistical significance, whereas the 10 N group effect was significant. These results identify a load-dependent wear-resistance trend under short-stroke dry sliding, but they remain a laboratory simplification. Actual Yangqin parts have non-ideal geometry, local impact, assembly clearance, possible lubrication and vibration coupling; these factors should be evaluated in future component-level tests before direct engineering application.

4. Conclusions

Within the scope of simplified ball-on-disk tests inspired by the wear-resistance requirements of Yangqin moving components, this study investigated USRP modification of 7075-T6 aluminum alloy. The results should be regarded as materials-level evidence for potential Yangqin applications rather than direct validation on real components.

1. By systematically studying the effects of static pressure, rolling speed, indentation depth and rolling passes on surface microstructure and properties, the selected USRP parameters were a rolling speed of 2000 mm/min, static pressure of 300 N, indentation depth of 0.10 mm and 8 rolling passes. Under these parameters, a continuous gradient nanostructured layer about 114 μm thick was formed, *Ra* decreased to (0.240 ± 0.009) μm, and near-surface hardness increased to (230 ± 14) HV. ANOVA confirmed significant group effects on *Ra*, *Rq* and near-surface hardness.

https://doi.org/10.64486/m.66.1.14

2. USRP treatment generally reduced mean COF and wear volume under both rotational and reciprocating laboratory sliding modes, although statistical significance depended on load and sliding mode. Rotational wear-volume differences were significant at 5 N and 10 N but not at 3 N. Reciprocating wear-volume differences were significant at 10 N but not at 3 or 5 N. The largest numerical wear-volume reductions were 40.9 % for rotational sliding at 5 N and 41.0 % for reciprocating sliding at 10 N. These results are relevant to, but not identical with, the motion of potential Yangqin-related components.
3. The untreated 7075 aluminum alloy is dominated by abrasive wear, characterized by deep furrows, material delamination and abundant hard wear debris. After USRP treatment, the dominant wear behavior changes toward adhesive wear accompanied by a compact mechanical mixing layer. TEM/HRTEM-based microstructural evidence, surface hardness improvement and the Hall-Petch grain-refinement effect jointly explain the enhanced wear resistance. Possible compressive residual stress introduced by USRP may also inhibit crack initiation and propagation, but direct XRD residual-stress measurement should be added in future work to quantify this effect.
4. The main limitation of this work is that the tests were performed on flat 7075 aluminum alloy samples rather than actual Yangqin components. Therefore, the present conclusions should be used as a basis for process selection and mechanism understanding. Further work should include representative Yangqin component geometry, realistic contact pairs, service loads, vibration/acoustic response and long-term durability validation.

References

[1] A. E. Sinin, S. Hamdan, C. Y. Jia, K. A. M. Said, and A. F. Musib, "The Yangqin: Acoustical study of a Chinese dulcimer," BioResources, vol. 21, no. 1, pp. 1084-1097, 2026. https://doi.org/10.15376/biores.21.1.1084-1097

[2] I. Argatov and Y. S. Chai, "Contact geometry adaptation in fretting wear: A constructive review," Front. Mech. Eng., vol. 6, Art. no. 51, 2020. https://doi.org/10.3389/fmech.2020.00051

[3] J. P. Nie, "Effect of Ultrasonic Surface Rolling Treatment on Friction and Wear Properties of 7075 Aluminum Alloy," Master's thesis, Guizhou University, Guiyang, China, 2024.

[4] M. Nakai and T. Eto, "New Aspect of Development of High Strength Aluminum Alloys for Aerospace Applications," Mater. Sci. Eng. A, vol. 285, nos. 1-2, pp. 62-68, 2000. https://doi.org/10.1016/S0921-5093(00)00667-5

[5] J. Liu and M. Kulak, "A New Paradigm in the Design of Aluminum Alloys for Aerospace Applications," Mater. Sci. Forum, vols. 331-337, pp. 127-142, 2000. https://doi.org/10.4028/www.scientific.net/MSF.331-337.127

[6] J. Xu, R. Qiu, K. Xia, et al., "The Surface Tribological Properties of 7075 Aluminum Alloy by HS-WEDM," in 2016 IEEE International Conference on Mechatronics and Automation, Harbin, China, pp. 1321-1326, 2016. https://doi.org/10.1109/ICMA.2016.7558754

[7] M. S. Surya and G. Prasanthi, "Effect of SiC Weight Percentage on Tribological Characteristics of Al7075/SiC Composites," Silicon, vol. 14, pp. 1083-1092, 2022. https://doi.org/10.1007/s12633-020-00885-5

[8] Y. Wang, Y. Yang, H. Yang, et al., "Effect of Nitriding on the Tribological Properties of Al1.3CoCuFeNi2 High-Entropy Alloy," J. Alloys Compd., vol. 725, pp. 365-372, 2017. https://doi.org/10.1016/j.jallcom.2017.07.132

[9] K. Edalati, A. Bachmaier, V. A. Beloshenko, et al., "Nanomaterials by Severe Plastic Deformation: Review of Historical Developments and Recent Advances," Mater. Res. Lett., vol. 10, no. 4, pp. 163-256, 2022. https://doi.org/10.1080/21663831.2022.2029779

[10] T. G. Langdon, "Processing by Severe Plastic Deformation: Historical Developments and Current Impact," Mater. Sci. Forum, vols. 667-669, pp. 9-14, 2011. https://doi.org/10.4028/www.scientific.net/MSF.667-669.9

[11] Z. Xiong, Y.-Z. Jiang, M. Yang, et al., "Achieving Superior Strength and Ductility in 7075 Aluminum Alloy through the Design of Multi-Gradient Nanostructure by Ultrasonic Surface Rolling and Aging," J. Alloys Compd., vol. 918, Art. no. 165669, 2022. https://doi.org/10.1016/j.jallcom.2022.165669

[12] Q. Sun, M. Yang, Y.-Z. Jiang, et al., "Achieving Excellent Corrosion Resistance Properties of 7075 Al Alloy via Ultrasonic Surface Rolling Treatment," J. Alloys Compd., vol. 911, Art. no. 165009, 2022. https://doi.org/10.1016/j.jallcom.2022.165009

[13] H. Ye, A. Chen, S. Liu, et al., "Effect of Ultrasonic Surface Rolling Process on the Surface Properties of QAl10-3-1.5 Aluminum Bronze Alloy," Surf. Coat. Technol., vol. 433, Art. no. 128126, 2022. https://doi.org/10.1016/j.surfcoat.2022.128126

[14] D. Chen, Y. Hu, L. Guo, et al., "The Modified Wear Resistance of Uranium Induced by Ultrasonic Surface Rolling Process," Wear, vols. 502-503, Art. no. 204390, 2022. https://doi.org/10.1016/j.wear.2022.204390

[15] P. Wang, H. Guo, D. Wang, et al., "Microstructure and Tribological Performances of M50 Bearing Steel Processed by Ultrasonic Surface Rolling," Tribol. Int., vol. 175, Art. no. 107818, 2022. https://doi.org/10.1016/j.triboint.2022.107818

[16] Z. Y. Zhou, G. L. Yu, Q. Y. Zheng, et al., "Wear Behavior of 7075 Aluminum after Ultrasonic-Assisted Surface Burnishing," J. Manuf. Process., vol. 51, pp. 1-9, 2020. https://doi.org/10.1016/j.jmapro.2020.01.026

[17] P. Zhang, K. H. Lee, and C. H. Lee, "Reciprocating Friction Characteristics of Magnetorheological Fluid for Aluminum under Magnetic Field," Trans. Nonferrous Met. Soc. China, vol. 24, no. 1, pp. 171-176, 2014. https://doi.org/10.1016/S1003-6326(14)63044-2

[18] N. Demoli, "Measuring Surface Vibrations of Musical Instruments Using an Inexpensive Digital Holography Device," Opt. Eng., vol. 44, no. 9, Art. no. 090502, 2005. https://doi.org/10.1117/1.2042467

[19] C.-H. Yin, Y.-L. Liang, Y. Liang, W. Li, and M. Yang, "Formation of a Self-Lubricating Layer by Oxidation and Solid-State Amorphization of Nano-Lamellar Microstructures during Dry Sliding Wear Tests," Acta Mater., vol. 166, pp. 208-220, 2019. https://doi.org/10.1016/j.actamat.2018.12.049

[20] J. Deng, W. Song, H. Zhang, et al., "Friction and Wear Behaviors of the Carbide Tools Embedded with Solid Lubricants in Sliding Wear Tests and in Dry Cutting Processes," Wear, vol. 270, nos. 9-10, pp. 666-674, 2011. https://doi.org/10.1016/j.wear.2011.01.031

https://doi.org/10.64486/m.66.1.14